ISSN 2706-655X Vol.3, Issue 7: 24-32, DOI: 10.25236/IJFET.2021.030705

Numerical Simulation of New Anode Baking Furnace

Li Han[a*], Yanfang Zhang[b], Yiwen Zhou[c], Yingtao Luo[d]

Zhengzhou Non-ferrous Metals Research Institute Co.Ltd of CHALCO, Zhengzhou, China
[a]hanli10.26@163.com, [b]zyy_zyf@rilm.com.cn, [c]zyy_zhyw@rilm.com.cn, [d]zyy_lyt@rilm.com.cn
**Corresponding author*

Abstract: *The quality of baked anode is directly determined by the uniformity of temperature field in the baking furnace flue-wall. The temperature difference between the upstream and downstream of the traditional furnace is large and the temperature distribution in the pit is uneven, and the natural gas energy consumption is high. In this work, the flow field in the flue and the temperature homogeneity in the pit of newly developed anode baking furnace are mainly presented. The industrial test in a carbon plant showed that a uniform temperature distribution is achieved and the quality of the baked anode is improved greatly with the natural gas saving of 10.4 m^3 per ton of carbon produced.*

Keywords: *Newly developed furnace, Numerical simulation, Temperature field, Homogeneity*

1. Introduction

In recent years, many scholars have carried out a large number of experiments and numerical simulation studies on anode baking furnace aiming to explore optimal solutions to anode baking performance [1-5]. However, this is very difficult, because there is not much room left for more tie-bricks, and the flow and temperature homogeneity are almost maximized. Also, this has been studied by many researchers who reached similar conclusion [6][7],in order to meet the need for further energy saving and consumption reduction of anode baking furnace for large-size anode blocks. But the research in China has just started on the development of a new anode baking furnace [8].

In the paper, the flow, the combustion, and heat transfer in the flue of the anode baking furnace are analyzed. The results of industrial tests indicate that the new anode baking furnace is superior to the traditional baking furnace. The results presented in this paper provide some insights into the structural optimization of carbon baking furnace.

2. Simulation model

2.1 Physical model

The ring anode baking furnace with 36 rooms, which is a part of a carbon plant, is analyzed. Considering the designs of the original and the new anode baking furnaces, two physical models are established separately. A 3D model was built comprising the firing section between the centerline of a pit and the centerline of a flue including the thickness of the flue-wall. In the pit, 21 anodes of 1550×660×660 mm in size are placed. The thickness of the flue wall is 100 mm. Symmetry was assumed on the centerline of the flue and the pit. Details of the model of new anode baking furnace are shown in Figure 1.

For simplification, the following factors are omitted in the simulation:

- The gas buoyancy in the fire flue.

- The heat loss caused by the infiltration and exfiltration of the air.

- The heat of combusting of the anode volatile matters.

- The filler coke between the flue-wall and anode.

It is assumed that:

- The inlet of air velocity and natural gas pressure are uniform.

ISSN 2706-655X Vol.3, Issue 7: 24-32, DOI: 10.25236/IJFET.2021.030705

- The natural gas combustion model is non-premixed, and the gas does not coexist with O_2.

- The heat generated by volatile combustion is considered in boundary conditions: inlet temperature of flue gas and the initial temperature of anode block

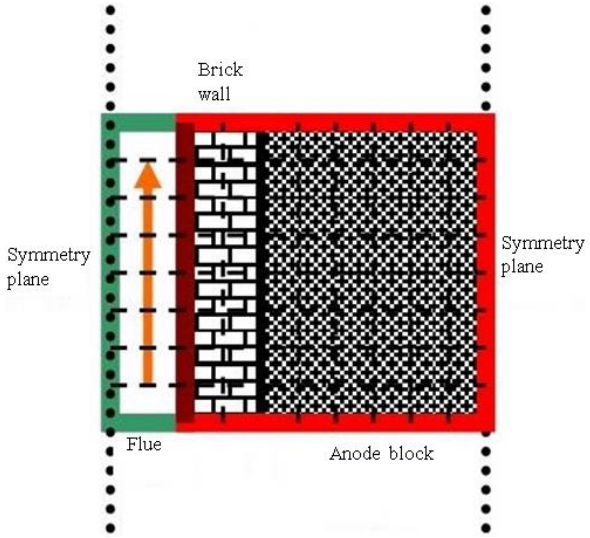

Figure 1. Cross-section Details of the 3D model in the present study (red: pit model, green: flue model, brown: interface).

2.2 Mathematical model

The mathematical model is the comprehensive governing equations of the main processes in the anode baking furnace, including the continuity equation, the momentum equation, energy equation, and component transport equation, etc.

2.2.1 The Continuity Equation

The description of incompressible gas flow is given as follow [9] [10]:

$$\nabla \cdot (\rho v) = 0 \tag{1}$$

where:

ρ Denotes gas density, kg/m^3

v Refers to the gas velocity, m/s

2.2.2 The Momentum Conservation Equations

Conservation of momentum in an inertial (non-accelerating) reference frame is described by

$$\rho(v \cdot \nabla)v = -\nabla p' + \nabla \cdot (\mu \nabla v) + \nabla \cdot (\mu \cdot (\nabla v)) \tag{2}$$

$$p' = p + \left(\frac{2}{3}\mu - \xi\right)\nabla \cdot v$$

$$\mu_{eff} = \mu + \mu_t$$

where:

p'Correction pressure, Pa

p Static pressure, Pa

ξ Volume viscosity coefficient

μ_{eff} Effective viscosity, Pa s

μ Molecular viscosity, Pa s

μ_t Is the turbulence viscosity, in the k-ε model turbulence viscosity $\mu_t = \frac{C_\mu \rho k^2}{\varepsilon}$,$C_\mu = 0.09$[9][10].

ISSN 2706-655X Vol.3, Issue 7: 24-32, DOI: 10.25236/IJFET.2021.030705

2.2.3 The Energy Equation

For steady state, the energy equation for the gas takes the following form:

$$\nabla \cdot \left(\vec{v}(\rho E + p)\right) = \nabla \cdot \left(k_{eff}\nabla T - \sum_j h_j \vec{J}_j + \left(\bar{\bar{\tau}}_{eff} \cdot \vec{v}\right)\right) + S_h \tag{3}$$

$$E = h - \frac{p}{\rho} + \frac{v^2}{2}$$

$$h = \sum_j Y_j h_j + \frac{p}{\rho}$$

$$h_j = \int_{Tref}^{T} c_{p,j}\, dT$$

The non-adiabatic non-premixed combustion model is enabled, the total enthalpy form of the energy equation:

$$\nabla \cdot (\rho \vec{v} H) = \nabla \cdot \left(\frac{k_{eff}}{c_p}\nabla H\right) + S_h \tag{4}$$

Where:

k_{eff} The effective conductivity ($k_t + k$, where k_t is the turbulent thermal conductivity, defined according to the turbulence model being used), W/m ·K

$\vec{J}_j$ The diffusion flux of speciesj, kg / (m2 s)

S_h The source term， including combustion reaction heat and radiant heat, W/m3

Y_j The mass fraction of species j, %

H The total enthalpy, J/kg

∇T The difference between the temperature of the flue gas and the reference temperature, K

C_p The specific heat of flue gas at constant pressure, J/kg ·K

In solid regions including the anode and the fire flue wall, the energy transport equation used by Fluent has the following form:

$$\frac{\partial}{\partial t}(\rho h) = \nabla \cdot (k \nabla T) \tag{5}$$

ρ The density of solid regions, kg/m3

h = sensible enthalpy, $h = \int_{T_{ref}}^{T} c_p\, dT$

T_{ref} The reference temperature, K

k The conductivity in the solid regions (anode, fire wall), W/m ·K [9] [10]

2.2.4 The P-1 Model Equation

The P-1 radiation model is the simplest case of the P-N model. The expression for $-\nabla q_r$ can be directly substituted into the energy equation to account for heat sources (or sinks) due to radiation.

$$-\nabla q_r = aG - 4an^2\sigma T^4 \tag{6}$$

The following equation is obtained for the radiation flux q_r:

$$q_r = -\frac{1}{3(a+\sigma_s)-C\sigma_s}\nabla G \tag{7}$$

Where:

a The absorption coefficient,

σ_s The scattering coefficient

G The incident radiation

ISSN 2706-655X Vol.3, Issue 7: 24-32, DOI: 10.25236/IJFET.2021.030705

C The linear-anisotropic phase function coefficient

n The refractive index of the medium

σ The Stefan-Boltzmann constant, 1.38×10-23J/K[10]

2.2.5 The Standard k-ε Model

The turbulence kinetic energy k and its rate of dissipation ε are obtained from the following transport equations:

$$\nabla(\rho v k) = \nabla\left[\left(\mu + \frac{\mu_T}{\sigma_k}\right)\cdot\nabla k\right] + G_k - \rho\varepsilon \tag{8}$$

and

$$\nabla(\rho v k) = \nabla\left[\left(\mu + \frac{\mu_T}{\sigma_\varepsilon}\right)\cdot\nabla\varepsilon\right] + \frac{C_{1\varepsilon}}{k}G_k - C_{2\varepsilon}\rho\frac{\varepsilon^2}{k} \tag{9}$$

In these equations, G_k represents the generation of turbulence kinetic energy due to the mean velocity gradients, calculated as described in Modeling Turbulent Production in the k-ε Models. $C_{1\varepsilon}$, $C_{2\varepsilon}$ and $C_{3\varepsilon}$ are constants. σ_k And σ_ε are the turbulent Prandtl numbers for k and ε respectively.

The turbulent (or eddy) viscosity μ_τ is computed by combining k and ε as follows:

$$\mu_\tau = \rho C_\mu \frac{k^2}{\varepsilon} \tag{10}$$

Where: C_μ is a constant [10]

2.2.6 The Transport Equation

The basis of the non-premixed modeling approach is that under a certain set of simplifying assumptions, the instantaneous thermochemical state of the fluid is related to a conserved scalar quantity known as the mixture fraction f.The mixture fraction can be written in terms of the atomic mass fraction as:

$$f = \frac{Z_i - Z_{i,Ox}}{Z_{i,fuel} - Z_{i,Ox}} \tag{11}$$

Where:

Z_i Elemental mass fraction for element i

$Z_{i,Ox}$ Mass fraction at the oxidizer stream inlet, %

$Z_{i,fuel}$ Mass fraction at the fuel stream inlet, %

The Favre mean (density-averaged) mixture fraction equation:

$$\nabla\cdot(\rho\vec{v}f) = \nabla\cdot\left(\left(\frac{k}{c_p} + \frac{\mu_t}{\sigma_t}\right)\nabla\bar{f}\right) \tag{12}$$

Where:

σ_t The Prandtl number

μ_t The turbulent viscosity [10]

3. Results and Discussions

3.1 Analysis of simulation results

3.1.1 Flow Field

Figure 2 shows the streamline and the velocity distribution of the gas flow in the flue of new anode baking furnace. The baffles are arranged without partitions, and the flue gas flow is significantly changed compared to that of the traditional baking furnace.

Figure 2 shows that the distribution of high-speed gas flow mainly is U-shaped in the flue, and yet the distribution of low-speed gas flow is mainly horizontal. At the back part of the baffles with several

ISSN 2706-655X Vol.3, Issue 7: 24-32, DOI: 10.25236/IJFET.2021.030705

key gaps, there exist several eddy regions (red rectangle) dominated by the burned gas from upstream nozzle, but the gas flow is obviously homogeneous behind the 5th column of baffles. The optimized gap between two baffles reasonably controls the flue gas flow and airflow along the shortest escaping path. On one hand, the gap leads to the uniformity of the high-temperature flue gas, and it maintains the relatively high temperature in the eddy region. On the other hand, it reasonably feeds oxygen helping the natural gas combustion of the third nozzle and minimizes the local higher temperature region caused by natural gas combustion near the 3rd peep hole.

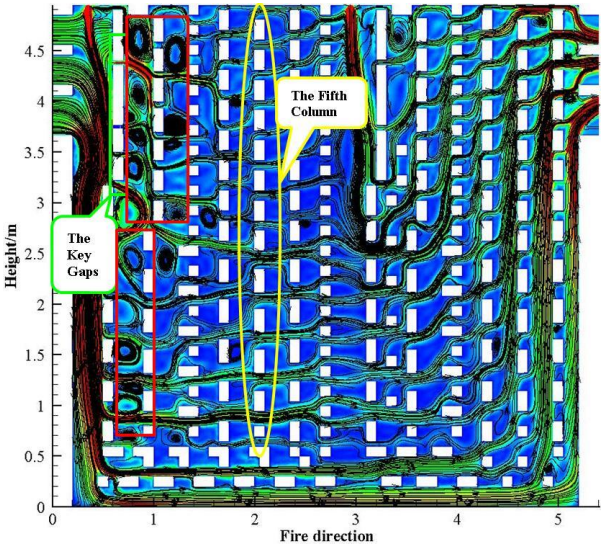

Figure 2.Gas flow streamlines and the velocity distribution of calculated result

3.1.2 Temperature Field

After the continuous improvement and optimization of the first version of new baking furnace, the better version of new baking furnace is obtained at present. The the followings figures are the comparison of the numerical simulation results between the traditional furnace and the new anode baking furnace. Figure 3 is the temperature distribution in central plane of the pit, and Figure 5 is the tendency of temperature distribution at 64 equidistant points in central plane of the pit.

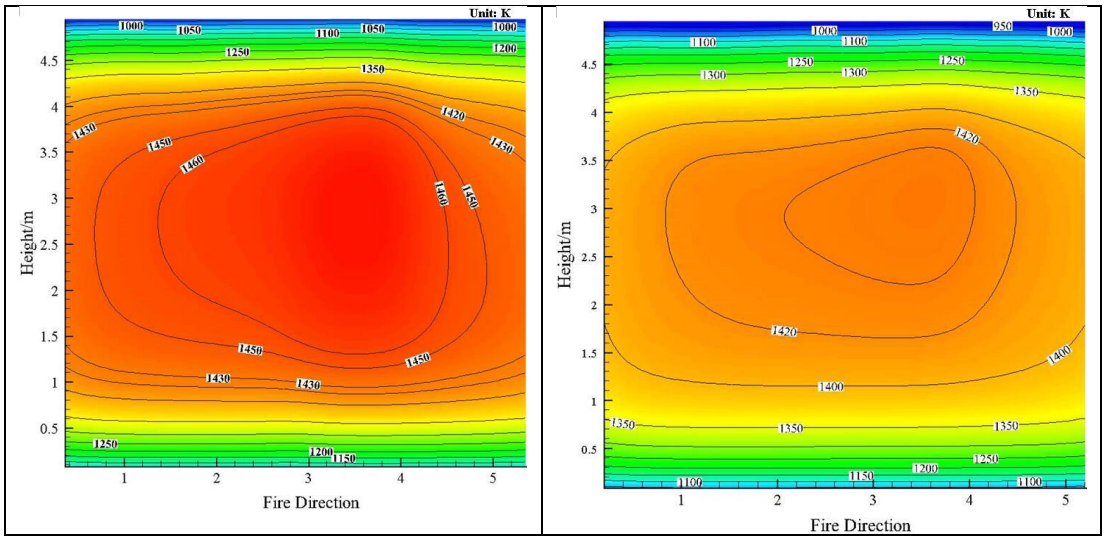

Figure 3. Calculated temperature map in the central plane of the pit. Left: traditional anode baking furnace, Right: newly developed anode baking furnace

ISSN 2706-655X Vol.3, Issue 7: 24-32, DOI: 10.25236/IJFET.2021.030705

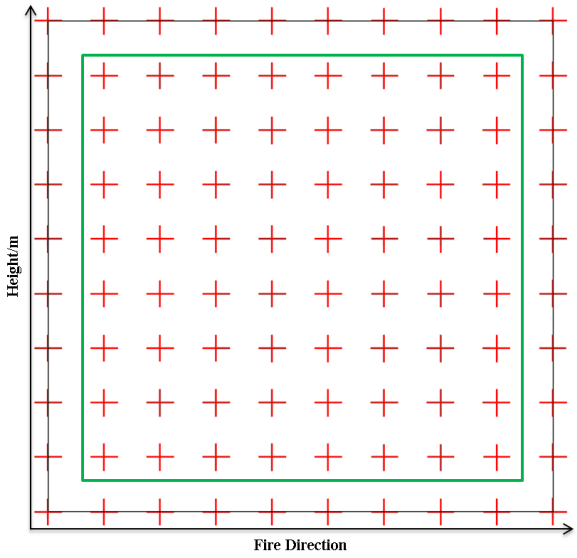

Figure 4. Distribution of equidistant points in central plane of pit (64 points in green square)

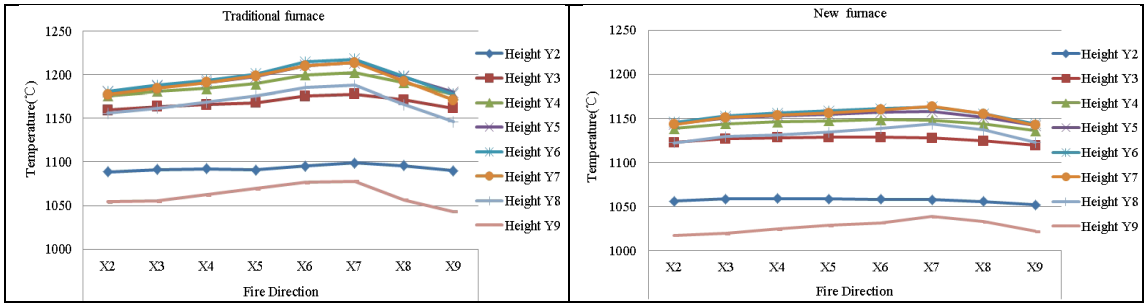

Figure 5. Distribution tendency of equidistant temperature points in central plane of pit.

Table 1. The analysis of equidistant points of the temperature data

	Traditional Furnace	New Furnace
Average temperature (℃)	1157.66	1117.90
Standard deviation (℃)	59.76	46.31
Maximum difference (℃)	195.39	145.28
External wall (W/m^2 Ƙ)	12.03	13.27

The arrangement of "W" type partitions forms the only passage for flue gas flow in the traditional fire flue and the temperature difference between upstream and downstream is relatively large. However, there is a small temperature difference between upstream and downstream in the newly developed baking furnace with optimized baffle arrangement based on the first version baking furnace. By balancing gaps between the baffles and providing more passages for the gas, the gas is well mixed which results in homogeneous gas temperature distribution in the flue.

Figure 3 shows at the same condition of feeding fuel, the pit temperature distribution of new anode baking furnace more unified, and the temperature gradient of the pit is smaller than that of traditional anode baking furnace. Figure 5 shows that the temperature curve of equidistant points is flatter than that of the traditional baking furnace. Table 1 shows that the temperature standard deviation of new anode baking furnace is 13.45℃ less than that of the convenction one and the maximum temperature difference is 50.11℃ lower by than that of the traditional anode baking furnace. However, the external convection heat transfer coefficient is 1.24W/m2 Ƙ higher and the heat dissipation is larger than that of traditional anode baking furnace. Consequently, the average peak temperature of the pit greatly drops 39.76℃, which is slightly lower than that of the traditional furnace.

The figures and the table indicate that the temperature homogeneity of the pit of new anode baking furnace greatly improves. However there is still room for further optimizing baffles of new anode baking furnace to increase the temperature of the whole pit at the same fuel input.

ISSN 2706-655X Vol.3, Issue 7: 24-32, DOI: 10.25236/IJFET.2021.030705

3.2 Comparison of calculated results and measured results

Figure 6 is the positions of temperature measurement points in the reference pit and the test pit. Reference pit refers to the pit in the traditional anode baking furnace and the test pit refers to the pit in the developed anode baking furnace.

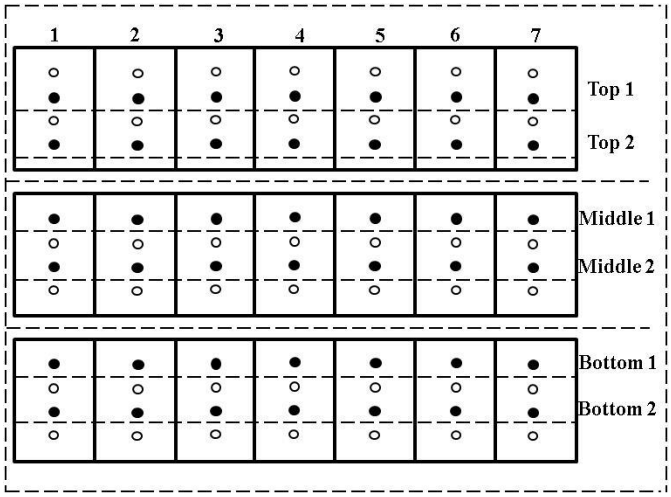

Figure 6. Distribution of measured temperature points

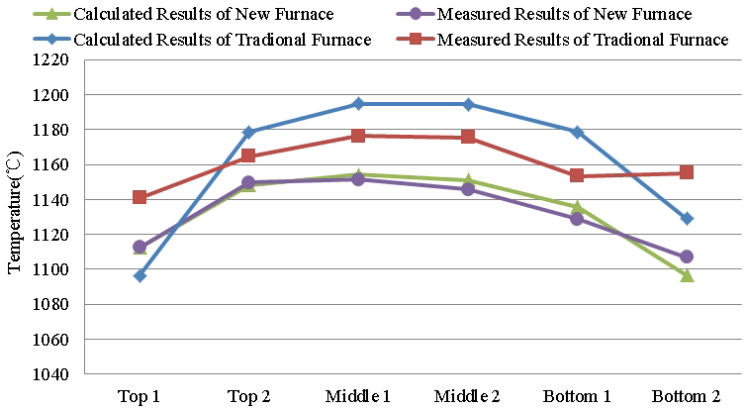

Figure 7. Comparison of the measured and measured average temperatures.

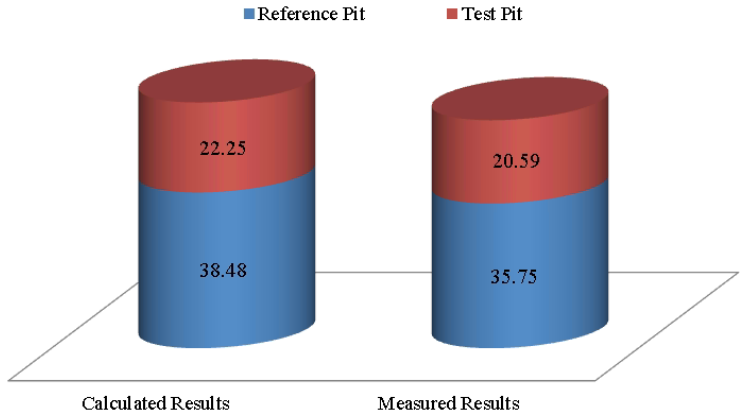

Figure 8. Comparison of the temperature standard deviation

Figure 7 and Figure 8 show that the measured results are consistent with calculated results. The lowest temperature locates at the bottom and upper part of the pit and the highest temperature locates in middle part of pit. The pit temperature of new anode baking furnace is slightly lower than that of the traditional anode baking furnace. The temperature standard deviation of the calculated result is 2.73℃ larger than that of the measured result in reference pit, in fact it is 1.66℃ in test pit. The difference of standard deviation of the calculated temperature is 16.23℃ between the test pit and the reference pit,

ISSN 2706-655X Vol.3, Issue 7: 24-32, DOI: 10.25236/IJFET.2021.030705

while that of the measured temperature is 15.16℃.

3.3 Industrial test results

3.3.1 The anode quality

Table 2 shows the physical and chemical indicators of anode samples of test pit and reference pit.

Table 2. Comparison of quality Parameters of the baked anode

Parameter	Density (kg/m^3)	Electrical resistivity (Ω m)	Compressive strength (MPa)	Flexural strength (MPa)	Air permeability Npm
Anode of test pit	1.582	56.54	41.4	10.4	1.89
Anode of reference pit	1.575	58.8	41.2	8.5	2.9

It can be seen from Table 2 that the density of the anode of the test pit increased by 7 g/m³, the average resistivity decreased by 2.26 Ω·m, and the air permeability decreased by 1.01 Npm. The anode quality has been significantly optimized and improved。

3.3.2 Natural gas consumption

In order to track the energy-saving effect of the newly developed furnace and the traditional furnace, the original burning frames are retrofitted; the natural gas consumption is measured. The detailed data on the natural gas consumption is shown in Table 3.

Table 3. The consumption of natural gas of the different furnace

The NO.	NO.23 furnace		NO.24 furnace		NO.25 furnace	
The result	Test flue	Reference flue	Test flue	Reference flue	Test flue	Reference flue
Total consumption (m^3)	2689	3565	3147	2731	1524	2649
Total gas saved (m^3)	876		-416		1125	
Gas saved per ton (m^3/t)	17.3		-8.2		22.2	
Average gas saved (m^3/t)	10.4					

Table 3 shows that of natural gas consumption per ton of carbon produced of the newly developed anode baking furnace is 10.4 m3 lower than that of traditional anode baking furnace in a production cycle, which indicates the energy-saving of the new furnace.

4. Conclusions

With the help of CFD software, the flow, temperature distribution and the temperature homogeneity of the pit of new anode baking furnace are studied. The high-temperature flue gas flow of the new furnace is mainly horizontal and the distribution of flow field is relatively uniform, which alleviates temperature differences between upstream and downstream. Moreover, the standard deviation (temperature homogeneity) of the pit of new furnace is better than that of traditional furnace.

The results show that the tendency of measured results are consistent with calculated results. The pit temperature homogeneity of the new anode baking furnace is better than that of the traditional furnace, and the performance of the baked anode is improved. The natural gas consumption per ton of anode of the new anode baking furnace is 10.4 m3 lower than that of the traditional one which indicates the energy saving and fuel consumption reduction.

References

[1] Severo D S，Gusberti V，Pinto E C V. Advanced 3D Modelling for anode baking furnace. Light metals 2005, 697-703.

[2] Chengjun Y, Minghou X．The numerical simulation of the improved combustion technology in an oil-fired anode baking furnace. Journal-Hua Zhong University of Science and Technology nature science Chinese edition (33) 2005, 13-16.

ISSN 2706-655X Vol.3, Issue 7: 24-32, DOI: 10.25236/IJFET.2021.030705

[3] Zhang L., Zheng C., Xu M., Simulating the heat transfer process of horizontal anode baking furnace. Dev. Chem.Eng. Mineral Process 12(3/4) 2004, 427-440.
[4] Felix Keller, Sierre, Ulrich Mannweiler, Dagoberto S. Severo. Computational Modeling in Anode Baking. R&D Carbon Ltd., Sierre, Switzerland, August 2006, 1-12.
[5] Dagoberto S. Severo. Recent developments in anode baking furnace design. Light Metals 2011, 853-858.
[6] Magali Gendre. A breakthrough in anode baking furnace flue-wall design. Light Metals 2007, 969-972.
[7] Yann El Ghaoui, Sandra Besson, Yannick Drouet. Anode baking furnace flue-wall design evolution: a return of experience of latest baffleless technology implementation. Light Metals 2016, 941-945.
[8] Yingtao Luo. A firewall structure of carbon baking furnace (in Chinese), CN108826990A, filed Sept. 5, 2018, granted October 25, 2019.
[9] Chengjun Yao, Minghou Xu. Simulation of flue combustion process in anode baking furnace (in Chinese). Journal of Huazhong University of science and technology (Nature Science Edition) (30) 2002, 60-62.
[10] ANSYS 19.2 Fluent Theory Guide.